

PAPER

Estimation of the infinitesimal generator by square-root approximation

To cite this article: Luca Donati *et al* 2018 *J. Phys.: Condens. Matter* **30** 425201

View the [article online](#) for updates and enhancements.

You may also like

- [TRANSIT TIMING OBSERVATIONS FROM KEPLER. I. STATISTICAL ANALYSIS OF THE FIRST FOUR MONTHS](#)
Eric B. Ford, Jason F. Rowe, Daniel C. Fabrycky *et al.*
- [A SEARCH FOR ADDITIONAL PLANETS IN THE NASA EPOXI OBSERVATIONS OF THE EXOPLANET SYSTEM GJ 436](#)
Sarah Ballard, Jessie L. Christiansen, David Charbonneau *et al.*
- [Structure Sensitivity of Electrochemical Reactions from First Principles: Applications to Nitrogen and Water Cycles](#)
Hee-Joon Chun, Siddharth Deshpande, Vesa Apaja *et al.*



IOP | ebooks™

Bringing together innovative digital publishing with leading authors from the global scientific community.

Start exploring the collection—download the first chapter of every title for free.

Estimation of the infinitesimal generator by square-root approximation

Luca Donati¹ , Martin Heida² , Bettina G Keller¹  and Marcus Weber³

¹ Department of Biology, Chemistry, Pharmacy, Freie Universität Berlin, Takustraße 3, 14195 Berlin, Germany

² Weierstrass Institute for Applied Analysis and Stochastics, Mohrenstr. 39, 10117 Berlin, Germany

³ Zuse Institute Berlin, Takustr. 7, 14195 Berlin, Germany

E-mail: luca.donati@fu-berlin.de, martin.heida@wias-berlin.de, bettina.keller@fu-berlin.de and weber@zib.de

Received 29 May 2018, revised 5 September 2018

Accepted for publication 7 September 2018

Published 3 October 2018



Abstract

In recent years, for the analysis of molecular processes, the estimation of time-scales and transition rates has become fundamental. Estimating the transition rates between molecular conformations is—from a mathematical point of view—an invariant subspace projection problem. We present a method to project the infinitesimal generator acting on function space to a low-dimensional rate matrix. This projection can be performed in two steps. First, we discretize the conformational space in a Voronoi tessellation, then the transition rates between adjacent cells is approximated by the geometric average of the Boltzmann weights of the Voronoi cells. This method demonstrates that there is a direct relation between the potential energy surface of molecular structures and the transition rates of conformational changes. We will show also that this approximation is correct and converges to the generator of the Smoluchowski equation in the limit of infinitely small Voronoi cells. We present results for a two dimensional diffusion process and alanine dipeptide as a high-dimensional system.

Keywords: infinitesimal generator, Markov state models, transfer operator, molecular kinetics, rate matrix

(Some figures may appear in colour only in the online journal)

1. Introduction

In recent decades, molecular processes, like conformational changes or binding processes, have been modeled and studied through molecular dynamics (MD) simulations. In MD simulations, one numerically solves the equation of motion of a molecule, in order to obtain a discretized trajectory, containing the position of each atom at each timestep. From a sufficiently large amount of MD trajectories, one can recover the Boltzmann distribution and estimate phase-space ensemble averages.

Under certain conditions, the dynamics of a molecular system can be studied as time evolution of probability densities $\rho_t(\mathbf{x})$ governed by the forward propagator, $\mathcal{P}(\tau)\rho_t(\mathbf{x}) = \rho_{t+\tau}(\mathbf{x})$, where τ is called lag time. The propagator has a unique stationary distribution $\pi(\mathbf{x})$, as long as

the underlying diffusion process is Markovian, ergodic and aperiodic.

Numerically easier to handle than the propagator is the closely related forward transfer operator [1–3] $\mathcal{T}(\tau)$, which propagates weighted probability densities $u_t(\mathbf{x}) = \rho_t(\mathbf{x})/\pi(\mathbf{x})$ forward in time

$$u_{t+\tau}(\mathbf{x}) = \mathcal{T}(\tau)u_t(\mathbf{x}). \quad (1)$$

Both the propagator and the transfer operator can be projected to finite dimensional matrices by a Galerkin discretization with respect to a set of ansatz functions $(\chi_1(\mathbf{x}), \chi_2(\mathbf{x}) \dots \chi_n(\mathbf{x}))$. If the ansatz functions are orthonormal, the Galerkin discretization of the transfer operator yields the matrix

$$\mathbf{T}(\tau) : T_{ij}(\tau) = \frac{\langle \chi_i | \mathcal{T}(\tau) \chi_j \rangle_\pi}{\langle \chi_i | \chi_i \rangle_\pi}, \quad (2)$$

where $\langle f|g \rangle_\pi = \int_\Gamma f(x) \cdot g(x) \pi(\mathbf{x}) d\mathbf{x}$. The denominator and the numerator can be interpreted as (time-lagged correlation) functions, $\langle \chi_i | \mathcal{T}(\tau) \chi_j \rangle_\pi = \text{cor}(\chi_j, \chi_i; \tau)$ and $\langle \chi_i | \chi_i \rangle_\pi = \text{cor}(\chi_i, \chi_i; \tau = 0)$, and can thus be estimated from a realization of the underlying diffusion process, i.e. from a trajectory produced by MD simulations.

A wide collection of methods have been developed to estimate the discretized version of the transfer operator from numerical simulations. The discretization can be carried out with respect to disjoint subsets of the conformational space (Markov state models [1–9]) or with respect to continuous functions of the state space (core-set Markov models [10], variational Markov models [11]). The dominant eigenvectors and associated eigenvalues of a Markov model contain information on long-lived molecular conformations, the kinetic exchange process between them and the associated equilibration times. This information can in turn be used to derive the hierarchy of barriers and minima of the underlying molecular free-energy surface. Markov models have been largely used in the last years and are now a fundamental tool to study and analyze the dynamics of molecular systems [12–17].

Associated to the transfer operator, there exists another operator called infinitesimal generator [2, 18]

$$\mathcal{Q} = \lim_{\tau \downarrow 0} \frac{\mathcal{T}(\tau) - \mathcal{T}(0)}{\tau}, \quad (3)$$

that defines the differential equation

$$\frac{\partial}{\partial t} u_t(\mathbf{x}) = \mathcal{Q} u_t(\mathbf{x}), \quad (4)$$

with solution

$$\begin{aligned} u_{t+\tau}(\mathbf{x}) &= \exp(\mathcal{Q}\tau) u_t(\mathbf{x}) \\ &= \mathcal{T}(\tau) u_t(\mathbf{x}). \end{aligned} \quad (5)$$

\mathcal{Q} and $\mathcal{T}(\tau)$ have the same eigenfunctions, while the eigenvalues of $\lambda_i(\tau)$ of $\mathcal{T}(\tau)$ are related to the eigenvalues θ_i of \mathcal{Q} , by

$$\lambda_i(\tau) = \exp(\tau \theta_i). \quad (6)$$

It follows that one can recover the same information about the dynamics of the system, both from the transfer operator and the generator.

The corresponding Galerkin discretization of the infinitesimal generator is called rate matrix, it provides a transition pattern in terms of rates between adjacent disjoint subsets of the conformational space. On the other hand, although several methods for the discretization of transfer operators are available, the discretized infinitesimal generator is more difficult to be estimated numerically, because it is not possible to derive the matrix elements of \mathbf{Q} from correlation functions. Furthermore, we will show in section 3 that there is no analogous relation of equation (5) for the discretized operators and then $\mathbf{T}(\tau) \neq \exp(\mathbf{Q}\tau)$ (see figure 1). This means that we cannot estimate \mathbf{Q} from $\tau^{-1} \log(\mathbf{T}(\tau))$.

We propose a method to discretize the infinitesimal generator based on a Voronoi partition of the conformational space. We start from the Galerkin discretization of the generator

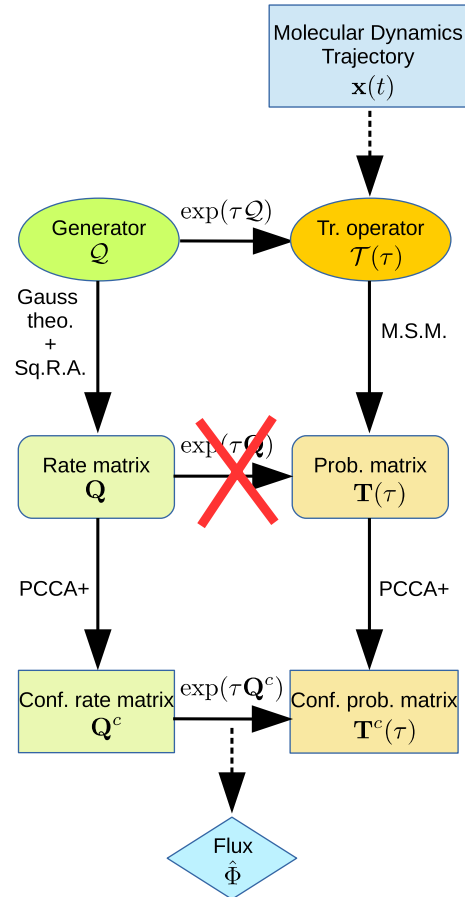


Figure 1. Scheme summarizing the theory of the transfer operator, the generator and the associated transition matrices.

$$\mathbf{Q} : Q_{ij} = \frac{\langle \chi_i | \mathcal{Q} \chi_j \rangle_\pi}{\langle \chi_i | \chi_i \rangle_\pi}, \quad (7)$$

where the ansatz functions are the characteristic functions of the Voronoi cells $\chi_i = \Omega_i$, i.e. a set of orthonormal functions. Then we derive a numerical scheme to estimate \mathbf{Q} that does not rely on correlation functions. Using the Gauss theorem, we write the rate between two neighboring cells in terms of the flux $\hat{\Phi}$ of configurations and of the Boltzmann weight of the intersecting surface between adjacent cells. Assuming that the flux is constant, we approximate the Boltzmann weight of the intersecting surface as the geometric average of the Boltzmann weight of the cells (square root approximation, SQRA), finding a direct algebraic relation between the potential energy function and the matrix elements Q_{ij} (equation (7)).

In principle, different types of averages (e.g. harmonic or arithmetic average) could be used, but a recently published proof [19] showed that the discretization of the generator converges, in the limit of infinitely small Voronoi cells, to the continuous infinitesimal generator \mathcal{Q} , if the Boltzmann weight of the intersecting surface is approximated by the geometric average. This SQRA has been used in literature before [20–22]. Interestingly, it cannot only be derived from the transition flux

density, but the same result has recently been obtained from the maximum path entropy principle [23].

The SQRA discretization closes an important gap in the discretization methods for dynamical operators. It is fundamentally different from the discretization methods for the transfer operator. The matrix elements Q_{ij} are not estimated from correlation functions, but are calculated from the Boltzmann weights of the cells Ω_i and Ω_j and a constant flux factor $\hat{\Phi}$.

Estimating Boltzmann weights tends to be much easier than estimating correlation functions. While for low-dimensional systems the Boltzmann weights can be estimated directly from the potential energy function, for high-dimensional systems, it is more convenient use the free energy profile on few relevant coordinates, which can be obtained from a wide range of enhanced sampling protocols. However, a method to estimate efficiently the constant flux $\hat{\Phi}$ has so far been lacking.

We are now able to apply the SQRA to realistic systems. Using a two dimensional diffusion process and alanine dipeptide as example of a high-dimensional system, we numerically test the initial assumptions of the method: Does the SQRA approximation yield the correct eigenspace of the system? Does the discretization error decrease in the limit of small Voronoi cells? Is the flux indeed constant and is it independent of the potential? Note that alanine dipeptide is a single amino acid, alanine, capped by two end groups. The end groups are chosen such that the central backbone torsion angles ϕ and ψ in alanine are subject to the same steric hindrances as an alanine residue within a longer peptide chain. This molecule thus serves as a standard test system for biomolecular dynamics simulations [6, 11, 24, 25].

In this paper, we give a detailed derivation of the SQRA, a summary of the proof that it converges to an infinitesimal generator in the limit of small Voronoi cells and we discuss the relations between operators described in figure 1. Next, we provide an approach to estimate the flux $\hat{\Phi}$ based on the robust Perron cluster analysis in conformation dynamics (PCCA+) [26].

2. Theory

We consider ergodic and reversible Markovian processes, whose dynamics can be represented by the forward transfer operator [1–3] $\mathcal{T}(\tau) : L^1_\pi(\Gamma) \rightarrow L^1_\pi(\Gamma)$, defined for a certain finite lag-time τ , that acts on relative probability densities $u_t(\mathbf{x}) = \rho_t(\mathbf{x})/\pi(\mathbf{x})$, where $\rho_t(\mathbf{x})$ is the probability density at time t and $\pi(\mathbf{x})$ is the stationary probability density. The transfer operator propagates the functions $u_t(\mathbf{x})$ forward in time according to

$$u_{t+\tau}(\mathbf{y}) = \mathcal{T}(\tau)u_t(\mathbf{y}) = \frac{1}{\pi(\mathbf{y})} \int_{\Gamma} p(\mathbf{x}, \mathbf{y}; \tau) u_t(\mathbf{x}) \pi(\mathbf{x}) d\mathbf{x}, \quad (8)$$

where $p(\mathbf{x}, \mathbf{y}; \tau)$ is the conditional probability to find the system in state \mathbf{y} , at time $t + \tau$, given that it was in the state \mathbf{x} at time t . The basis of our considerations is a discretization of the state space Γ into disjoint subsets Ω_i . The Galerkin discretization $\mathcal{T}(\tau)$ (equation (2)) with respect to these subsets, turns into a row-stochastic transition matrix $\mathbf{T}(\tau)$. Its

dominant eigenvectors, approximations of the eigenfunctions of $\mathcal{T}(\tau)$, contain information about the dynamics of the dominant processes of the system [1–7, 9], associated with a timescale defined as:

$$t_i(\tau) = -\frac{\tau}{\ln(\lambda_i(\tau))}, \quad \forall \tau > 0, \quad (9)$$

where $\lambda_i(\tau)$ is the i th eigenvalue of the matrix $\mathbf{T}(\tau)$. If $t_i(\tau)$ does not depend on the lag time τ , then the matrix $\mathbf{T}(\tau)$ satisfies the Markovian property [3, 5] and the discretization is considered valid, i.e. the underlying discretized molecular process can be approximated as a Markov chain with time step τ in this discretized space. In this case t_i is the implied timescale at which the i th dominant process occurs.

Besides the transition matrix $\mathbf{T}(\tau)$, we can also define a rate matrix \mathbf{Q} , which is in the same sense a discretization of the infinitesimal generator \mathcal{Q} of the transfer operator. The infinitesimal generator and the transfer operator are related by

$$\begin{aligned} \mathcal{Q}f(\mathbf{x}) &= \left. \frac{\partial \mathcal{T}(\tau)}{\partial \tau} \right|_{\tau=0} f(\mathbf{x}) \\ &= \lim_{\tau \downarrow 0} \frac{\mathcal{T}(\tau) - \mathcal{T}(0)}{\tau} f(\mathbf{x}), \end{aligned} \quad (10)$$

whose solution is

$$\mathcal{T}(\tau) = \exp(\mathcal{Q}\tau). \quad (11)$$

Because the eigenvalues of \mathcal{Q} and $\mathcal{T}(\tau)$ are related by equation (6), the implied timescales of the kinetic processes can be derived also from the eigenvalues θ_i of the rate matrix:

$$t_i = -\frac{1}{\theta_i}. \quad (12)$$

Note that the implied timescales derived from the eigenvalues of the rate matrix (equation (12)) do not depend on the lag time. In the next section, we will show how to discretize the infinitesimal generator \mathcal{Q} , into a rate matrix \mathbf{Q} , following Lie *et al* [21].

2.1. Square root approximation

Consider a Voronoi tessellation of the state space $\Gamma = \cup_{i=1}^n \Omega_i$, then define the transition probability matrix $\mathbf{T}(\tau)$, via equation (2), the entries $T_{ij}(\tau)$ describe the probability to jump from the cell Ω_i to the cell Ω_j in a time span τ . The associated infinitesimal generator can be discretized on the basis of the same tessellation (equation (7)). Formally, the transition probability matrix and the rate matrix are related by $\mathbf{Q} := \left. \frac{\partial \mathbf{T}(\tau)}{\partial \tau} \right|_{\tau=0}$. Using the Gauss theorem one can show that the non-diagonal entries of the matrix satisfy

$$Q_{ij} = \frac{1}{\pi_i} \oint_{\partial\Omega_i \partial\Omega_j} \Phi(\mathbf{z}) \pi(\mathbf{z}) dS(\mathbf{z}), \quad (13)$$

where $\partial\Omega_i \partial\Omega_j$ is the common surface between the cell Ω_i and Ω_j , π_i is the Boltzmann probability of the cell Ω_i and $\Phi(\mathbf{z})$ denotes the flux of the configurations \mathbf{z} through the infinitesimal surface $\partial\Omega_i \partial\Omega_j$. The complete derivation is provided in appendix A.

Multiplying and dividing the matrix entries Q_{ij} (equation (13)) by the Boltzmann density of the intersecting surface $\partial\Omega_i\partial\Omega_j$

$$s_{ij} = \oint_{\partial\Omega_i\partial\Omega_j} \pi(\mathbf{z}) \, dS(\mathbf{z}), \quad (14)$$

one obtains

$$\begin{aligned} Q_{ij} &= \frac{s_{ij}}{\pi_i} \oint_{\partial\Omega_i\partial\Omega_j} \Phi(\mathbf{z}) \frac{\pi(\mathbf{z})}{s_{ij}} dS(\mathbf{z}) \\ &= \frac{s_{ij}}{\pi_i} \langle \Phi \rangle_{ij}, \end{aligned} \quad (15)$$

where $\langle \Phi \rangle_{ij}$ represents the mean value of the flux through the surface $\partial\Omega_i\partial\Omega_j$.

In what follows, we make the following assumptions.

1. The flux $\hat{\Phi}$ is constant and does not depend on the potential energy function, it holds $\hat{\Phi} = \langle \Phi \rangle_{ij}$.
2. The cells are so small such that $\pi(\mathbf{x})$ is almost constant on every cell Ω_i and on every interface $\partial\Omega_i\partial\Omega_j$, i.e. $\pi|_{\Omega_i} \approx \pi_i$ and $\pi|_{\partial\Omega_i\partial\Omega_j} \approx \pi_{ij}$.

Due to assumption 1, the matrix elements of \mathbf{Q} can be rewritten as

$$Q_{ij} = \frac{s_{ij}}{\pi_i} \hat{\Phi}. \quad (16)$$

The quantity s_{ij} (equation (17)), i.e. the Boltzmann density of the intersecting surface between two neighboring cells Ω_i and Ω_j , is a surface integral that can be approximated by the Boltzmann density π_{ij} due to assumption 2:

$$\begin{aligned} s_{ij} &= \oint_{\partial\Omega_i\partial\Omega_j} \pi(\mathbf{z}) dS(\mathbf{z}) \\ &\approx \pi_{ij}. \end{aligned} \quad (17)$$

Thus equation (16) reads

$$Q_{ij} = \frac{\pi_{ij}}{\pi_i} \hat{\Phi}. \quad (18)$$

A second approximation is necessary to estimate the Boltzmann weight of the intersecting surface π_{ij} . We have chosen to use the geometric mean of the Boltzmann weights of the centers of the cells Ω_i and Ω_j , which corresponds to an arithmetic mean of the corresponding potential energy function of the cells:

$$\begin{aligned} \pi_{ij} &= \sqrt{\pi_i \pi_j} \\ &= \exp\left(-\beta \frac{V(\Omega_i) + V(\Omega_j)}{2}\right). \end{aligned} \quad (19)$$

In principle, other mean-value calculations could be used, but as we will show in the next section, only by the geometric mean the discretized operator converges to the continuous infinitesimal generator. Finally, the entries of the rate matrix are written as

$$Q_{ij} = \frac{\sqrt{\pi_i \pi_j}}{\pi_i} \hat{\Phi} = \sqrt{\frac{\pi_j}{\pi_i}} \hat{\Phi}. \quad (20)$$

Note that it is not necessary to know the partition function of the system, because it would cancel in the ratio π_j/π_i in

equation (20). Thus the unnormalized Boltzmann weights π_i and π_j can be used.

The matrix \mathbf{Q} , as formulated in equation (20), is a valid approximation of the infinitesimal generator \mathcal{Q} (equation (10)), that satisfies the properties of a rate matrix:

1. The diagonal entries satisfy $Q_{ii} = -\sum_{j \neq i} Q_{ij}$.
2. The sum of the rows is zero $\sum_j Q_{ij} = 0$.

Moreover, the matrix \mathbf{Q} defines the master equation for a jump process

$$\left. \frac{\partial \rho_i}{\partial \tau} \right|_{\tau=0} = C \sum_{i \sim j} (\rho_j Q_{ji} - \rho_i Q_{ij}), \quad (21)$$

where ρ is the probability density, C is a normalization constant and the notation $i \sim j$ denotes neighboring cells.

2.2. Convergence of the rate matrix

The square root approximation of the infinitesimal generator \mathcal{Q} is based on a Voronoi tessellation of the state space. In principle, it is not clear if this kind of approximation has a physically meaningful limit, whenever the number of Voronoi cells tends to infinity. If this limit exists, it is furthermore not clear whether the limit operator is physically reasonable. An arbitrary refinement strategy of increasing the number of Voronoi cells will probably not converge. However, a recent mathematical study [19] which will be published separately, shows that under suitable assumptions on the Voronoi tessellation, the square root approximation converges towards the generator of the Smoluchowski equation, i.e. towards the Langevin dynamics for the limit of high friction.

In what follows, let ε denote the maximal diameter of the cells and for given $\varepsilon > 0$ let $(P_i^\varepsilon)_i$ be the set of points that generate the Voronoi tessellation and let Ω_i^ε be the Voronoi cell that corresponds to P_i^ε . For any continuous function ρ , we write $\rho_i^\varepsilon := \rho(P_i^\varepsilon)$. In particular, for the function $\pi(x) := \exp(-\beta V(x))$ we write $v_i^\varepsilon := \sqrt{\pi_i^\varepsilon}$ and using equation (20) we denote the right hand side of equation (21) as

$$(\mathcal{L}^\varepsilon \rho)_i^\varepsilon := C_\varepsilon \sum_{i \sim j} \left(\rho_j^\varepsilon \frac{v_i^\varepsilon}{v_j^\varepsilon} - \rho_i^\varepsilon \frac{v_j^\varepsilon}{v_i^\varepsilon} \right), \quad (22)$$

where $\sum_{i \sim j}$ relates to the sum over all neighboring cells Ω_j^ε of the cell Ω_i^ε and where we interpret $(\mathcal{L}^\varepsilon \rho)_i^\varepsilon$ as a function which is constant on every Ω_i^ε . Written in a formal way, for the scaling factor $C_\varepsilon = \varepsilon^{-2}$ and a suitable positive definite symmetric matrix $A_{\text{hom}} \in \mathbb{R}^{n \times n}$, it holds for twice continuously differentiable functions u that [19]

$$\begin{aligned} C_\varepsilon \sum_{i \sim j} \left(\rho_j^\varepsilon \frac{v_i^\varepsilon}{v_j^\varepsilon} - \rho_i^\varepsilon \frac{v_j^\varepsilon}{v_i^\varepsilon} \right) &\rightarrow \nabla \cdot (A_{\text{hom}} \nabla \rho(x)) \\ &+ \beta \nabla \cdot (\rho(x) A_{\text{hom}} \nabla V(x)) \quad \text{as } \varepsilon \rightarrow 0, \end{aligned} \quad (23)$$

provided that $P_i^\varepsilon \rightarrow x$ as $\varepsilon \rightarrow 0$. In case that the Voronoi tessellations are isotropic, we find $A_{\text{hom}} = a\mathbb{I}$, where $a > 0$ is a constant and \mathbb{I} is the identity. However, if for some reason the tessellations are systematically anisotropic, the right hand side

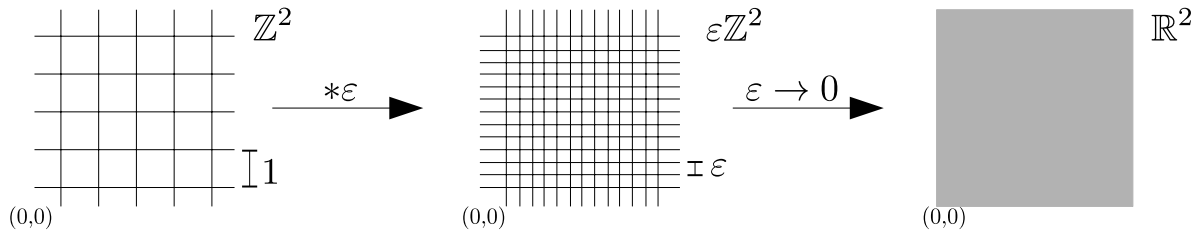


Figure 2. The role of the parameter in the case $\varepsilon\mathbb{Z}^2$. As $\varepsilon \rightarrow 0$, the grid becomes finer and finer and approximates the whole of \mathbb{R}^2 .

of equation (23) can be brought into the form of a classical Fokker–Planck operator via a coordinate transform. Hence, we also call the right hand side of equation (23) a Fokker–Planck operator. In what follows, we will roughly explain how the convergence (23) can be obtained.

There exists a simpler version of equation (22) known as the discrete Laplace operator \mathcal{F}^ε having the form

$$(\mathcal{F}^\varepsilon \rho)_i^\varepsilon := C_\varepsilon \sum_{i \sim j} (\rho_j^\varepsilon - \rho_i^\varepsilon). \quad (24)$$

Note that the use of \mathcal{L} and \mathcal{F} is opposite in [19]. It turns out that the understanding of the asymptotic behavior of \mathcal{F}^ε is essential for the study of the asymptotic behavior of \mathcal{L}^ε .

In case the point process is a rectangular grid (figure 2), the operator \mathcal{F}^ε has been studied intensively and in broad generality from physicists (as generator of a Markovian process that models Brownian motion, see the review [27]) and mathematicians (for rigorous results, see the review [28]). The notion of discrete Laplace operator can be understood as follows: On the lattice $\varepsilon\mathbb{Z}^n$ (that consists of all points $x \in \mathbb{R}^n$ such that $(\varepsilon^{-1}x) \in \mathbb{Z}^n$, see figure 2), the discrete derivative in the j th direction is given by $d_{j,\varepsilon}\rho(x) := \frac{1}{\varepsilon}(\rho(x + \varepsilon e_j) - \rho(x))$, where e_j is the j th unit vector. The second order discrete derivative is given by

$$\begin{aligned} d_j^2 \rho(x) &:= \frac{1}{\varepsilon} (d_j \rho(x) - d_j \rho(x - \varepsilon e_j)) \\ &= \frac{1}{\varepsilon^2} [(\rho(x + \varepsilon e_j) - \rho(x)) + (\rho(x - \varepsilon e_j) - \rho(x))]. \end{aligned} \quad (25)$$

Hence, we obtain for $x_i^\varepsilon \in \varepsilon\mathbb{Z}^n$ that

$$\sum_{j=1}^n d_j^2 \rho(x_i^\varepsilon) = \varepsilon^{-2} \sum_{j \sim i} (\rho(x_j^\varepsilon) - \rho(x_i^\varepsilon)) = (\mathcal{F}^\varepsilon \rho)_i, \quad (26)$$

where now $i \sim j$ relates to all neighbors $x_j^\varepsilon \in \varepsilon\mathbb{Z}^n$ of x_i^ε s.t. $|x_j^\varepsilon - x_i^\varepsilon| = \varepsilon$. We now show that for twice continuously differentiable functions u , it holds

$$(\mathcal{F}^\varepsilon \rho)_i^\varepsilon \rightarrow \Delta \rho \quad \text{as } \varepsilon \rightarrow 0 \text{ if } x_i^\varepsilon \rightarrow x. \quad (27)$$

In order to show this, we use Taylor’s formula, i.e.

$$\rho(x + \varepsilon e_i) - \rho(x) = \partial_i \rho(x) \varepsilon + \frac{1}{2} \partial_i^2 \rho(x) \varepsilon^2 + \sum_{k=3}^{\infty} \frac{1}{k!} \partial_i^k \rho(x) \varepsilon^k \quad (28)$$

and hence

$$\begin{aligned} d_j^2 \rho(x_i^\varepsilon) &= \frac{1}{\varepsilon^2} \left(\partial_j \rho(x_i^\varepsilon) \varepsilon + \frac{1}{2} \partial_j^2 \rho(x_i^\varepsilon) \varepsilon^2 + \sum_{k=3}^{\infty} \frac{1}{k!} \partial_j^k \rho(x_i^\varepsilon) \varepsilon^k \right) \\ &\quad + \frac{1}{\varepsilon^2} \left(-\partial_j \rho(x_i^\varepsilon) \varepsilon + \frac{1}{2} \partial_j^2 \rho(x_i^\varepsilon) \varepsilon^2 + \sum_{k=3}^{\infty} \frac{1}{k!} \partial_j^k \rho(x_i^\varepsilon) (-\varepsilon)^k \right) \\ &= \partial_j^2 \rho(x_i^\varepsilon) + \mathcal{O}(\varepsilon). \end{aligned} \quad (29)$$

From this, we obtain that equation (27) holds.

We will now use the above insights to formally understand the asymptotic behavior of the operator

$$(\mathcal{L}^\varepsilon \rho)_i := \varepsilon^{-2} \sum_{i \sim j} \left(\rho_j^\varepsilon \frac{v_i^\varepsilon}{v_j^\varepsilon} - \rho_i^\varepsilon \frac{v_j^\varepsilon}{v_i^\varepsilon} \right),$$

$$\text{where } v_i^\varepsilon = \exp\left(-\frac{1}{2}\beta V(x_i^\varepsilon)\right), \quad (30)$$

on the lattice $\varepsilon\mathbb{Z}^n$. Writing $V_i^\varepsilon := V(x_i^\varepsilon)$ and using the Taylor’s formula, we obtain

$$\frac{v_i^\varepsilon}{v_j^\varepsilon} = 1 - \frac{1}{2}\beta (V_i^\varepsilon - V_j^\varepsilon) + \frac{1}{8}\beta^2 (V_i^\varepsilon - V_j^\varepsilon)^2 - \mathcal{O}\left((V_i^\varepsilon - V_j^\varepsilon)^3\right) \quad (31)$$

and inserting this expansion into equation (30), we obtain

$$\begin{aligned} (\mathcal{L}^\varepsilon \rho)_i &= \varepsilon^{-2} \sum_{i \sim j} \left((\rho_j^\varepsilon - \rho_i^\varepsilon) + \frac{\beta}{2} (\rho_j^\varepsilon + \rho_i^\varepsilon) (V_j^\varepsilon - V_i^\varepsilon) \right) \\ &\quad + \varepsilon^{-2} \sum_{i \sim j} \left(\frac{1}{8}\beta^2 (V_i^\varepsilon - V_j^\varepsilon)^2 + \mathcal{O}\left((V_i^\varepsilon - V_j^\varepsilon)^4\right) \right) (\rho_j^\varepsilon - \rho_i^\varepsilon) \\ &\quad + \varepsilon^{-2} \sum_{i \sim j} (\rho_j^\varepsilon + \rho_i^\varepsilon) \mathcal{O}\left((V_i^\varepsilon - V_j^\varepsilon)^3\right). \end{aligned} \quad (32)$$

We know that for small $\varepsilon \approx 0$, it holds $(V_i^\varepsilon - V_j^\varepsilon) \approx \varepsilon \nabla V(x_i^\varepsilon) + \mathcal{O}(\varepsilon^2)$ and equivalently $(\rho_i^\varepsilon - \rho_j^\varepsilon) \approx \varepsilon \nabla \rho(x_i^\varepsilon) + \mathcal{O}(\varepsilon^2)$. Therefore, we obtain

$$(\mathcal{L}^\varepsilon \rho)_i^\varepsilon = \varepsilon^{-2} \sum_{i \sim j} \left((\rho_j^\varepsilon - \rho_i^\varepsilon) + \frac{\beta}{2} (\rho_j^\varepsilon + \rho_i^\varepsilon) (V_j^\varepsilon - V_i^\varepsilon) \right) + \mathcal{O}(\varepsilon) \quad (33)$$

and using once more the Taylor expansion for u and V in equation (33), we further obtain

$$\begin{aligned} (\mathcal{L}^\varepsilon \rho)_i^\varepsilon &= \varepsilon^{-2} \sum_{i \sim j} (\rho_j^\varepsilon - \rho_i^\varepsilon) + \varepsilon^{-2} \rho_i^\varepsilon \sum_{i \sim j} \beta (V_j^\varepsilon - V_i^\varepsilon) \\ &\quad + \varepsilon^{-2} \sum_{i \sim j} \frac{\beta}{2} (\rho_j^\varepsilon - \rho_i^\varepsilon) (V_j^\varepsilon - V_i^\varepsilon) + \mathcal{O}(\varepsilon) \\ &= \varepsilon^{-2} \sum_{i \sim j} (\rho_j^\varepsilon - \rho_i^\varepsilon) + \varepsilon^{-2} \rho_i^\varepsilon \sum_{i \sim j} \beta (V_j^\varepsilon - V_i^\varepsilon) \\ &\quad + \sum_{i \sim j} \frac{\beta}{2} \partial_j \rho(x_i^\varepsilon) \cdot \partial_j V(x_i^\varepsilon) + \mathcal{O}(\varepsilon). \end{aligned} \quad (34)$$

Thus, as $\varepsilon \rightarrow 0$ we observe that

$$\begin{aligned} (\mathcal{L}^\varepsilon \rho)_i^\varepsilon &\rightarrow \Delta \rho(x) + \beta \rho(x) \Delta V(x) + \beta \nabla \rho(x) \cdot \nabla V(x) & x_i^\varepsilon &\rightarrow x \\ &= \Delta \rho(x) + \beta \nabla \cdot (\rho(x) \nabla V(x)) \end{aligned}$$

on the grid $\varepsilon \mathbb{Z}^n$. Hence, we recover equation (23) with $A_{\text{hom}} = 1$ for the cubic Voronoi tessellation.

On arbitrary Voronoi tessellations, things become more involved. In particular, the convergence (equation (27)) or calculations like in equations (29) and (34) do not hold anymore, as they rely on the rectangular structure of \mathbb{Z}^n . However, the key ideas of the proof remain the same with the difference that some terms which explicitly cancel out in the above calculation only vanish in a ‘statistically averaged’ sense, using G-convergence.

G-convergence is a concept from early stage in the development of Homogenization theory and is rarely used (refer to [29]), since other concepts are usually much better suited. In the discrete setting, G-convergence can be formulated in the following sense: The operator \mathcal{F}^ε is called G-convergent if there exists a symmetric positive definite matrix A_{hom} such that for every continuous $f : \Omega \rightarrow \mathbb{R}$ the sequence ρ^ε of solutions to

$$-(\mathcal{F}^\varepsilon \rho^\varepsilon)_i := -\sum_{j \sim i} (\rho_j^\varepsilon - \rho_i^\varepsilon) = f(P_i^\varepsilon), \quad (35)$$

converges in $L^2(\Omega)$ to the solutions ρ of $-\nabla \cdot (A_{\text{hom}} \nabla \rho) = f$, where we interpret ρ^ε as a function that is constant on every cell Ω_i^ε . Hence, G-convergence and convergence of the SQRA-operator are more or less equivalent conditions on the tessellation. In recent years, G-convergence (or equation (27)) has been proved for random operators

$$(\mathcal{F}_{\omega}^\varepsilon \rho)(x_i) := \frac{1}{\varepsilon^2} \sum_{j \sim i} \omega_{ij} (\rho(x_j) - \rho(x_i)) \quad (36)$$

on the grid $\varepsilon \mathbb{Z}^n$ for a broad range of random coefficients ω_{ij} (see the overview in [28]). However, for stationary and ergodic tessellations, the recent results in [19, 30] seem to be the only ones.

In conclusion, we showed that the convergence in equation (23) holds on the rectangular grid for sufficiently smooth functions ρ . The calculations suggest that the result also holds on more general grids. However, on such more general grids, the mathematics behind the convergence (equation (23)) becomes much more involved and is thus shifted to the article [19]. The results there, are though more general as they state that solutions of $\mathcal{L}^\varepsilon \rho^\varepsilon = f^\varepsilon$ converge to solutions of $\mathcal{L} \rho = f$ provided $f^\varepsilon \rightarrow f$ in $L^2(Q)$.

3. Discretization error

3.1. Relation between transition probability and rate matrices

The Markovian property of the transition probability matrix $\mathbf{T}(\tau)$, i.e. the discretized version of the transfer operator $\mathcal{T}(\tau)$, is guaranteed only by a proper discretization of the space [3, 31, 32]. For example, assume a discretization of the space into three disjoint sets A , B , and C . If the system is in the state

$\mathbf{x} \in A$, it will jump to a set B or C with different probabilities, depending on the position inside the set A . Because the position inside the set A depends on the previous position, the Markovian property is lost, on the level of the set A .

Note that a fine enough discretization of the space prevents the loss of the Markovian property. Alternatively, it can be proven that for a large enough value of the lag time τ , the Chapman–Kolmogorov condition $\mathbf{T}(n \cdot \tau) = \mathbf{T}(\tau)^n$ holds [3], guarantying the Markovianity of the process.

With regard to the matrix \mathbf{Q} , two problems arise.

- If τ is too small, the matrix $\mathbf{T}(\tau)$ could not describe a Markovian process and the matrix \mathbf{Q} cannot be considered a proper generator of $\mathbf{T}(\tau)$.
- If τ is large enough to guarantee the Markovianity of $\mathbf{T}(\tau)$, then the generator \mathbf{Q} is the correct generator, but it is not physically meaningful. A proper generator is defined for $\tau \rightarrow 0$, in other words for instantaneous transitions that occur between neighboring sets. If τ is too big, then \mathbf{Q} would describe instantaneous transition rates between non-neighboring sets, that are not physical if we are considering a time-continuous dynamics.

In conclusion, the matrix \mathbf{Q} , obtained by square root approximation (equation (20)) is the Galerkin discretization of the infinitesimal generator \mathcal{Q} , but it is not the correct generator of the transition probability matrix $\mathbf{T}(\tau)$.

3.2. Flux estimation

The entries of the matrix \mathbf{Q} (equation (20)) are written as the product of the term $\tilde{Q}_{ij} = \sqrt{\frac{\pi_j}{\pi_i}}$ and the flux $\hat{\Phi}$ that is assumed to be constant:

$$Q_{ij} = \sqrt{\frac{\pi_j}{\pi_i}} \cdot \hat{\Phi} = \tilde{Q}_{ij} \cdot \hat{\Phi}.$$

While the first term can be estimated analytically from the potential energy function of the system, the factor $\hat{\Phi}$ is unknown. Thus, we can estimate only the matrix \mathbf{Q} , that represents the correct rates up to the scaling factor $\hat{\Phi}$. Nonetheless, the eigenvectors of the matrix \mathbf{Q} are a correct approximation of the eigenfunctions of the continuous operator \mathcal{Q} , while the eigenvalues θ_i , are scaled by the factor $\hat{\Phi}$ as well, such that $\theta_i \approx \theta_i \cdot \hat{\Phi}$, where θ_i are the correct eigenvalues of \mathcal{Q} .

Because the eigenvalues of the transfer operator $\lambda_i(\tau)$ are associated to the eigenvalues of the infinitesimal generator θ_i by the relation

$$\exp(\tau \theta_i) = \lambda_i(\tau) \quad \forall i > 1, \quad (37)$$

one could estimate the value of the flux, by comparing the eigenvalues of the rate matrix $\tilde{\mathbf{Q}}$, with the eigenvalues of the matrix $\mathbf{T}(\tau)$ obtained by MSM. Unfortunately, because the matrix \mathbf{Q} is not the correct infinitesimal generator of $\mathbf{T}(\tau)$, following this route would lead to a wrong result.

Molecular systems are characterized by n_c conformations in the space, i.e. metastable subsets of the state space where the system stays for a time significantly longer than some macroscopic time span. The matrices \mathbf{Q} and $\mathbf{T}(\tau)$ can be

reduced to the $n_c \times n_c$ matrices of the conformations \mathbf{Q}^c and $\mathbf{T}^c(\tau)$ that satisfy

$$\exp(\tau \mathbf{Q}^c) = \mathbf{T}^c(\tau). \quad (38)$$

Thus, the flux can be obtained from the eigenvalues of the matrices of the conformations. The derivation and the mathematical proof of equation (38) is given in the appendix B.

Here, we propose a simple scheme to estimate $\hat{\Phi}$ based on equation (38). Firstly, one constructs the matrix $\tilde{\mathbf{Q}}$ by SQRA and the matrix $\mathbf{T}(\tau)$ by MSM. Afterward, the two matrices are reduced respectively to $\tilde{\mathbf{Q}}^c$ and $\mathbf{T}^c(\tau)$ by PCCA+ and the flux is estimated from the respective eigenvalues as

$$\hat{\Phi}_i = \frac{\log \lambda_i^c(\tau)}{\tau \tilde{\theta}_i^c} \quad \forall i \in (1, n_c). \quad (39)$$

In equation (39) the subscript i denotes that the flux $\hat{\Phi}_i$ has been estimated from the i th pair of eigenvalues $\{\lambda_i^c(\tau), \tilde{\theta}_i^c\}$. Actually, $\hat{\Phi}$ should not depend on the choice of the eigenvalues, but, in our numerical experiments, different values of $\hat{\Phi}_i$ have been found for different pairs of eigenvalues. The result improves, i.e. the difference reduces, if the Voronoi cells are more homogeneously distributed. Thus, estimating the flux from different eigenvalues (equation (39)), and the respective standard deviation can be used as a test to evaluate the quality of the SQRA.

4. Methods

4.1. Two dimensional system

We consider the two-dimensional diffusion process governed by the stochastic differential equation:

$$\begin{cases} dx_t = -\nabla_x V(x_t, y_t) + \sigma dB_t^x \\ dy_t = -\nabla_y V(x_t, y_t) + \sigma dB_t^y \end{cases}, \quad (40)$$

where B_t^i denotes a standard Brownian motion in the direction $i = x, y$, σ is the volatility and $V(x_t, y_t)$ is a two-dimensional potential energy surface given by the function:

$$V(x, y) = 4 \left(x^3 - \frac{3}{2}x \right)^2 - x^3 + x + 2 + 2y^2. \quad (41)$$

In principle, we could estimate the rate matrix of the system by SQRA, with no need to integrate the equation of motion. We could generate a set of random points uniformly distributed on \mathbb{R}^2 , then discretize the space by a Voronoi tessellation and apply the SQRA formula (equation (20)). On the other hand, only a subset of \mathbb{R}^2 is relevant for the dynamics of the system, thus we solve numerically the equation of motion in order to sample the conformational space. A discretized trajectory is also useful to build a MSM and to estimate a correct value of the flux.

We have numerically integrated equation (40) with the Euler–Maruyama scheme, producing trajectories of 4×10^7 time-steps with a time step $\Delta t = 0.001$, for several values of the volatility σ .

Afterward, we have partitioned the sampled space with a Voronoi tessellation, picking random points from the

trajectories, such that the minimum distance between two points, is the distance r , an input parameter that represents the minimum diameter of the cells. Both the parameter r and the volatility σ affect the quality of the Voronoi tessellation and the number of cells. A simulation at high volatility, samples a larger subset of the state space, thus the Voronoi cells are more homogeneously distributed and approximately of the same size. We have produced trajectories with $\sigma = 1.0, 1.5, 2.0, 2.5$ and built Voronoi tessellation with $r = 0.1, 0.15, 0.2$.

We point out that it is not necessary to know the complete Voronoi tessellation to build the SQRA, but only the adjacency matrix that identifies the neighboring cells. Thinking of the Voronoi diagram in terms of convex polyhedra [21, 33] permits to write a linear program to estimate the adjacency matrix, improving the efficiency compared to usual algorithms.

To estimate the flux of the system, we have constructed MSMs with enforced detailed balance [34] for each trajectory. The MSMs have been constructed on the same tessellation used for the SQRA, choosing a lag time range from 100 to 1000 time steps.

The PCCA+ analysis has been realized using three conformations as input parameter.

To study the dependence of the flux on the potential energy, we have perturbed the potential energy function (equation (41)) with the function

$$U(\kappa, x) = \kappa x \quad (42)$$

where κ is a parameter that tunes the strength of the perturbation.

4.2. Alanine dipeptide

We studied alanine dipeptide in explicit water, built as acetyl-alanine-methylamide (Ac-A-NHMe) capped with an acetyl group on the N-terminus and n-methylamide on the C-terminus (Ac-Ala-NHMe), in order to simulate the dynamics of the torsion angles within a peptide chain.

The rate matrix has been constructed on the two relevant coordinates, the backbone torsion angles ϕ and ψ . Thus, the potential energy function $V(\mathbf{x})$ has been replaced by the free energy profile $F(\phi, \psi)$ on torsion angles in the SQRA formula. Because an analytical function for $F(\phi, \psi)$ is unknown, a MD simulation was necessary to estimate the free energy profile from the histogram of the trajectory projected on ϕ and ψ .

We carried out simulations with the GROMACS 5.0.2 simulation package [35], with the force field AMBER ff-99SB-ildn [36] and the TIP3P water model [37]. A velocity rescale thermostat [38] has been applied to control the temperature and a leap-frog integrator [39] has been used to integrate the equation of the motion with a timestep of 2 fs. We have performed simulations in a NVT ensemble, at temperature of 300 and 900 K. The length of each simulation was 600 ns and we printed out the positions every $nstxout = 500$ time steps, corresponding to 1 ps.

The space on relevant coordinates $\{\phi, \psi\} = [-\pi, \pi] \times [-\pi, \pi]$ has been discretized with a $2\pi \times 2\pi$ -periodic Voronoi tessellation. To study the quality of the SQRA as a

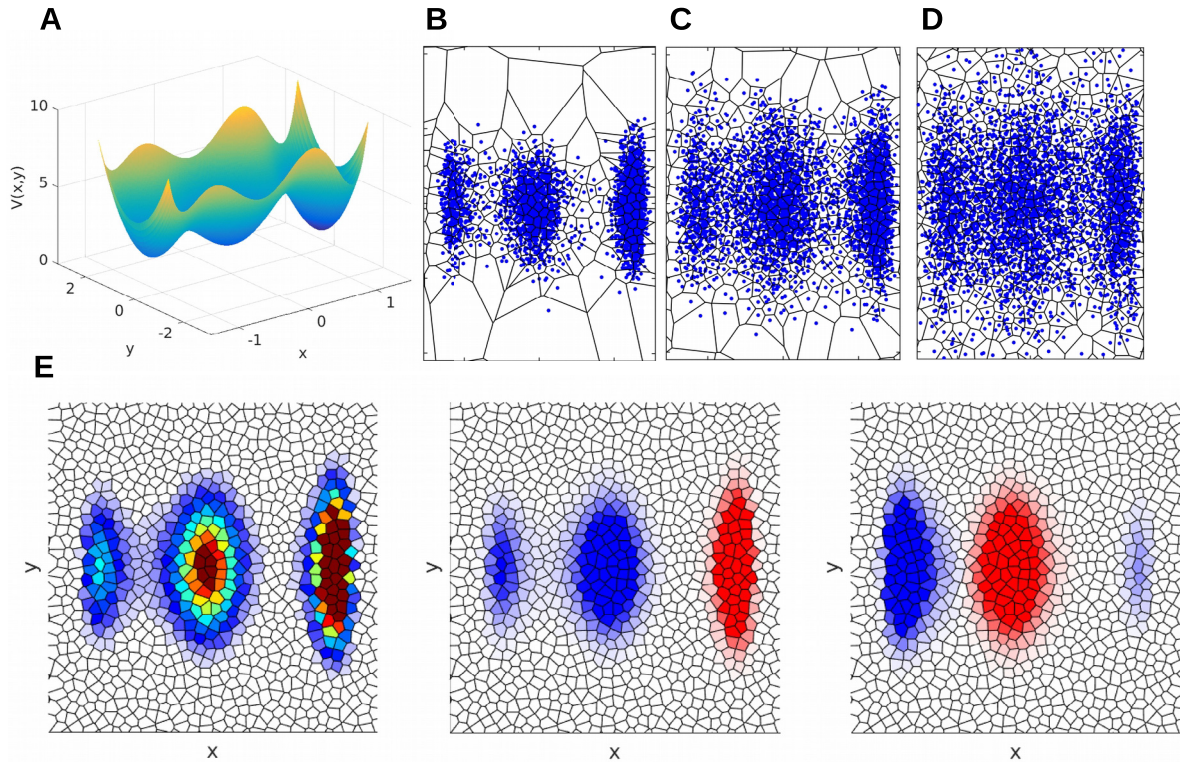


Figure 3. Two-dimensional system. (A) Potential energy function. (B) Trajectory generated with $\sigma = 1.0$. (C) Trajectory generated with $\sigma = 1.5$. (D) Trajectory generated with $\sigma = 2.0$. (E) First three left eigenvectors of the rate matrix.

function of the size of the cells, we used as minimum diameter $r = 0.1, 0.14, 0.17$ rad.

The trajectories used to sample the free energy profile has been used also to build the MSMs and to estimate the flux. The MSMs have been built with enforced detailed balance on the same Voronoi tessellation of the rate matrix, with a lag-time range of [0:300] ps.

5. Results and discussion

5.1. Two-dimensional system

As first application, we illustrate the method for a two-dimensional diffusion process. The potential energy function (equation (41), figure 3(A)) has three minima respectively at $(-1.12, 0)$, $(0.05, 0)$ and $(1.29, 0)$, separated by two barriers, whose highest points are approximately at $(-0.83, 0)$ and $(0.61, 0)$.

Because the potential energy function is known and the system is two-dimensional, one could build the discretized generator by SQRA, without producing any trajectory, but using random points uniformly distributed on the space \mathbb{R}^2 . This approach is not possible for high-dimensional systems, in which the accessible state space, at a given temperature T , makes up only a small fraction of the total state space. In high-dimensional systems, the accessible state space has to be identified by a molecular simulation. Therefore we have numerically solved the equation of motion to produce a discretized trajectory of the two dimensional system and sample the most characteristic states of the space. Moreover, we used

the trajectory to select random states as centers of the Voronoi cells Ω_i , whose Boltzmann weight π_i have been estimated as arithmetic mean of the unnormalized Boltzmann densities of all the points of the trajectory falling in the cell Ω_i :

$$\pi_i = \left(\sum_{k=1}^{\text{nsteps}} \mathbf{1}_{\Omega_i}(x_k, y_k) \right)^{-1} \cdot \sum_{k=1}^{\text{nsteps}} \mathbf{1}_{\Omega_i}(x_k, y_k) \exp(-\beta V(x_k, y_k)) \quad \forall \text{cell } \Omega_i, \quad (43)$$

where $\{x_k, y_k\}$ are the coordinates of the k th point of the trajectory, $\mathbf{1}_{\Omega_i}(x_n, y_n)$ is the indicator function of the Voronoi cell Ω_i and nsteps is the length of the trajectory. The quantity $\sum_{k=1}^{\text{nsteps}} \mathbf{1}_{\Omega_i}(x_k, y_k)$ represents the number of times that the trajectory has visited the cell Ω_i .

We first discuss the results obtained from a simulation with volatility $\sigma = 2.0$ and a partition of the space in 1725 Voronoi cells, realized with $r = 0.1$ as minimum diameter of the cells (figure 3(D)).

Figure 3(E) shows the first three left eigenvectors of the matrix $\tilde{\mathbf{Q}}$, i.e. of the matrix \mathbf{Q} scaled by the factor $\hat{\Phi}$. The first left SQRA eigenvector, associated to the eigenvalue $\theta_1 = 0$ has only positive entries and represents the Boltzmann distribution. The dominant eigenvectors, associated to eigenvalues $\theta_i < 0$, have positive and negative values and represent kinetic exchanges between regions with different sign. In particular, the second eigenvector describes the slowest kinetic process between the region that includes the first and second minimum (blue area in figure 3(E)) and the third minimum (red area in figure 3(E)), through the highest barrier of the potential energy function. The third eigenvector represents the second slowest transition, between the middle minimum

Table 1. Two-dimensional system. First five eigenvalues and implied timescales as function of the flux. The volatility was set equal to 1.5 and the minimum distance between the centers of neighbor cells was set equal to $r = 0.1$.

i	θ_i	ITS (time steps)
1	0	—
2	-0.0142	$70.5319\hat{\Phi}^{-1}$
3	-0.0522	$19.1482\hat{\Phi}^{-1}$
4	-0.0738	$13.5452\hat{\Phi}^{-1}$
5	-0.0871	$11.4772\hat{\Phi}^{-1}$
6	-0.1252	$7.9900\hat{\Phi}^{-1}$

Table 2. Two-dimensional system. Ratio ITS_i/ITS_j between the first five implied timescales of table 1. The volatility was set equal to 1.5 and the minimum distance between the centers of neighbor cells was set equal to $r = 0.1$.

$i \backslash j$	2	3	4	5	6
2	1.00	3.68	5.20	6.14	8.82
3	0.27	1.00	1.41	1.66	2.39
4	0.19	0.70	1.00	1.18	1.69
5	0.16	0.59	0.84	1.00	1.43
6	0.11	0.41	0.58	0.69	1.00

and the two on the sides. All the other eigenvectors (data not shown) describe faster dynamic exchanges inside the metastable regions. The left SQRA eigenvectors are in great agreement with the left MSM eigenvectors (data not shown) and are an excellent approximation of the eigenfunctions of the infinitesimal generator.

The respective eigenvalues θ_i of the generator are associated to the eigenvalues of the transfer operator (equation (6)) and contain information about the implied timescales associated to the kinetic processes of the system. Thus, from the eigenvalues of the rate matrix, we can obtain a valid approximation of the implied timescales of the system according to equation (12). The advantage of estimating the implied timescales from the eigenvalues of the rate matrix (equation (12)), respect to the eigenvalues of the transition probability matrix (equation (9)), is that it is not necessary to verify the convergence of the implied timescales as in MSMs [3]. On the other hand, if we do not know the value of $\hat{\Phi}$, then we can only know the eigenvalues $\tilde{\theta}_i$ of the matrix $\tilde{\mathbf{Q}}$, that are correct up to the scaling factor $\hat{\Phi}$. The eigenvalues $\tilde{\theta}_i$ are useful anyway to evaluate how much a dominant process is faster than another one. For example, if the second eigenvector is associated to a timescale of $t_2 = 70.53\hat{\Phi}^{-1}$ time steps, while the third eigenvector is associated to a timescale of $t_3 = 19.14\hat{\Phi}^{-1}$ time steps, then the process associated to the third eigenvector is 3.68 times faster than the process associated to the second eigenvector (tables 1 and 2).

5.2. Estimation of the flux

To estimate the value of the flux $\hat{\Phi}$, we have built MSMs and the matrices of the conformations $\tilde{\mathbf{Q}}^c$ and $\mathbf{T}^c(\tau)$ by PCCA+. Because the system has three metastable states, the matrices

Table 3. Two-dimensional system. Variation of the flux as function of the volatility σ . The minimum distance between the centers of neighbor cells was set equal to $r = 0.1$.

σ	ncells	$\hat{\Phi}_2$	$\hat{\Phi}_3$	$\bar{\Phi}$	std	rel. err. (%)
1.0	740	0.0080	0.0161	0.0121	0.0057	47.11
1.5	1258	0.0461	0.0523	0.0492	0.0044	8.94
2.0	1725	0.0913	0.0931	0.0922	0.0013	1.41
2.5	2205	0.1427	0.1372	0.1400	0.0039	2.79

Table 4. Two-dimensional system. Variation of the flux as function of the minimum distance between the centers of neighbor cells. The volatility was set equal to 2.0.

r	ncells	$\hat{\Phi}_2$	$\hat{\Phi}_3$	$\bar{\Phi}$	std	rel. err. (%)
0.20	456	0.0207	0.0248	0.0227	0.0029	12.87
0.15	784	0.0396	0.0425	0.0410	0.0021	5.12
0.10	1725	0.0913	0.0931	0.0922	0.0013	1.41

$\tilde{\mathbf{Q}}^c$ and $\mathbf{T}^c(\tau)$ are 3×3 and the flux $\hat{\Phi}$ has been estimated comparing the second and third eigenvalues of the matrices, i.e. $\{\tilde{\theta}_i^c, \lambda_i^c(\tau); i = 2, 3\}$. In each table that we present (tables 3–6), $\hat{\Phi}_2$ denotes the flux estimated comparing the second eigenvalues, $\hat{\Phi}_3$ denotes the flux estimated comparing the third eigenvalues, $\bar{\Phi}$ is the average flux between $\hat{\Phi}_2$ and $\hat{\Phi}_3$, ‘std’ is the standard deviation and ‘rel. err.’ is the relative error.

We have first studied how the flux depends on the volatility of the system, then we have produced four trajectories respectively with $\sigma = 1.0, 1.5, 2.0$ and 2.5 and built four rate matrices by SQRA and four transition probability matrices by MSM. The Voronoi tessellation of the space has been realized with $r = 0.15$. The trajectories for $\sigma = 1.0, \sigma = 1.5$ and $\sigma = 2.0$ and the respective partitions of the space are presented in figures 3(B)–(D).

Increasing the volatility, that is linked to the temperature of the environment, the trajectory samples a larger subset of the state space. Because the Voronoi tessellation is realized by picking random points from the trajectories, at high volatility, the tessellation consists of a large number of cells, homogeneously distributed and approximately of the same size. The average flux increases linearly with the volatility (table 3, col. $\hat{\Phi}$), because high volatility corresponds to a faster dynamics: a given cell is visited for a short amount of time, consequently, the number of times that a cell border is crossed rises. We also observe that the error on the flux, i.e. the difference between $\hat{\Phi}_2$ and $\hat{\Phi}_3$ reduces significantly increasing the volatility (table 3, column ‘rel. err.’). Thus, we deduce that the quality of the SQRA is intrinsically linked to the quality of the Voronoi tessellation and the error on the measure reduces when the cells are homogeneously distributed.

Afterward, we have studied how the flux depends on the size of the cells (parameter r , table 4). Keeping the volatility constant ($\sigma = 2.0$), but reducing the minimum distance between centers ($r = 0.2, 0.15$ and 0.1), a single cell is visited for a shorter time and the number of transitions through the intersecting surface, i.e. the flux, grows. We also note a

Table 5. Two-dimensional system. Variation of the flux as function of an external perturbation. The volatility was set equal to 1.5 and $r = 0.1$.

κ	ncells	$\hat{\Phi}_2$	$\hat{\Phi}_3$	$\bar{\Phi}$	std	rel. err. (%)
0.0	1258	0.0461	0.0523	0.0492	0.0044	8.94
0.5	1235	0.0459	0.0502	0.0480	0.0030	6.25
1.0	1225	0.0449	0.0526	0.0487	0.0055	11.29

significant reduction of the relative error, that confirms the convergence of the rate matrix to the continuous generator for small Voronoi cells.

Finally, we have studied how a perturbation (equation (42) with $\kappa = 0, 0.5, 1$) of the potential energy function affects the flux. The effect of such perturbation is to tilt the potential energy function along the axis x and to modify respectively the Boltzmann weights. The experiment has been repeated with $\sigma = 1.5$ and $\sigma = 2.0$ and the results are collected respectively in tables 5 and 6. In both the cases the perturbation does not affect the average flux, confirming the initial assumption that the flux does not depend on the potential energy function.

5.3. Alanine dipeptide

As high dimensional system, we have studied alanine dipeptide (Ac-A-NHMe) in explicit water. In principle, one could estimate the rate matrix using the full potential energy function, that is parametrized by the forcefield [36], but the resulting high-dimensional rate matrix would be computationally intractable. We have constructed the rate matrix and the MSM on two relevant coordinates, the backbone dihedral angles ϕ and ψ , that capture the main dynamical properties of the system. Running a MD simulation was necessary only to sample the free energy landscape, which can be recovered by a normalized histogram of a long trajectory projected on the dihedral angles ϕ and ψ . If the two-dimensional space $\{\phi, \psi\}$ is discretized by a Voronoi tessellation, then the Boltzmann weight of each cell is proportional to the number of times that the system has visited the cell Ω_i divided by the length of the trajectory:

$$\pi_i(\phi, \psi) = \lim_{\text{nsteps} \rightarrow +\infty} \frac{\sum_{k=1}^{\text{nsteps}} \mathbf{1}_{\Omega_i}(\phi_k, \psi_k)}{\text{nsteps}} \quad \forall \text{cell } \Omega_i \quad (44)$$

where $\{\phi_k, \psi_k\}$ are the coordinates of the system at time step k and nsteps is the length of the trajectory. Consequently, the free energy profile of the cell Ω_i reads

$$F_i(\phi, \psi) = -\frac{1}{k_B T} \log \pi_i(\phi, \psi) + C, \quad (45)$$

where C is a negligible constant.

We have first studied the rate matrix built on free energy profile obtained from a simulation at 300 K. In this case, the MD simulation does not sample the full state space and large regions of the space $\{\phi, \psi\}$, are never visited (figures 4(A) and (B)). In particular, few trajectory points are found in the barrier regions at $\phi \sim 0$, resulting large Voronoi cells in these regions. We have built the Voronoi tessellation, on

Table 6. Two-dimensional system. Variation of the flux as function of an external perturbation. The volatility was set equal to 2.0 and $r = 0.1$.

κ	ncells	$\hat{\Phi}_2$	$\hat{\Phi}_3$	$\bar{\Phi}$	std	rel. err. (%)
0.0	1725	0.0913	0.0931	0.0922	0.0013	1.41
0.5	1722	0.0927	0.0922	0.0924	0.0003	0.36
1.0	1720	0.0904	0.0926	0.0915	0.0015	1.64

the same trajectory, with $r = 0.1$ (figure 4(A)) and $r = 0.17$ (figure 4(B)). In both the cases the cells have significant different sizes in the minima and barrier regions. The only way to improve the discretization, i.e. to have small cells homogeneously distributed, is to increase the temperature to permit a better sampling of the state space. Figure 4(C) shows a trajectory at temperature 900 K, that covers a larger subspace of the state space, with a much more homogeneous Voronoi tessellation. From the two-dimensional system and from alanine dipeptide, we have learnt that simulations at high temperatures (high volatilities), yield a homogeneous Voronoi discretization. Furthermore, at high temperatures the flux can be estimated with much higher confidence, than at low temperatures. This suggests that the Voronoi discretization for the SQRA should be based on a high temperature simulation, even if the goal is to model the dynamics at room temperature. The realistic magnitude of the implied timescales can be estimated from the high temperature simulation in a second step. Indeed, the Boltzmann weights can be obtained from the high temperature simulation by first calculating the free energy profile via equation (45) and then converting F_i into the Boltzmann weights at room temperature via equation (46). In summary, we propose a strategy in which a model of the dynamics at room temperature is obtained entirely from a simulation at high temperature.

Figure 4(D) shows the dominant left eigenvectors of the rate matrix built on the trajectory sampled at 900 K. The first eigenvector represents the Boltzmann distribution with the typical conformational states (β region, L_α region, and R_α region). The second eigenvector represents a kinetic exchange between the L_α -minimum ($\phi > 0$) and the α -helix and β -sheet minima ($\phi < 0$). The associated implied timescale is $146\hat{\Phi}^{-1}$ ps. The third eigenvector represents a transition β -sheet \longleftrightarrow α -helical conformation, i.e. a torsion around ψ , and is associated to a timescale of $40\hat{\Phi}^{-1}$ ps. The eigenvectors are the same obtained from a MSM [25].

Even though the free energy profile was built on a trajectory produced at temperature $T = 900$ K, the eigenvectors are a valid approximation of the eigenvectors of the system at $T = 300$ K. Indeed, the simulation at $T = 900$ K was used only to build the free energy profile according to equation (45), but the Boltzmann weights for the SQRA have been estimated by the approximation

$$\pi_i \approx \exp(-\beta F_i(\phi, \psi)) \quad (46)$$

where $\beta = \frac{1}{k_B T}$ has been set after the simulation with $T = 300$ K. Instead of this simple approximation to get the free energy

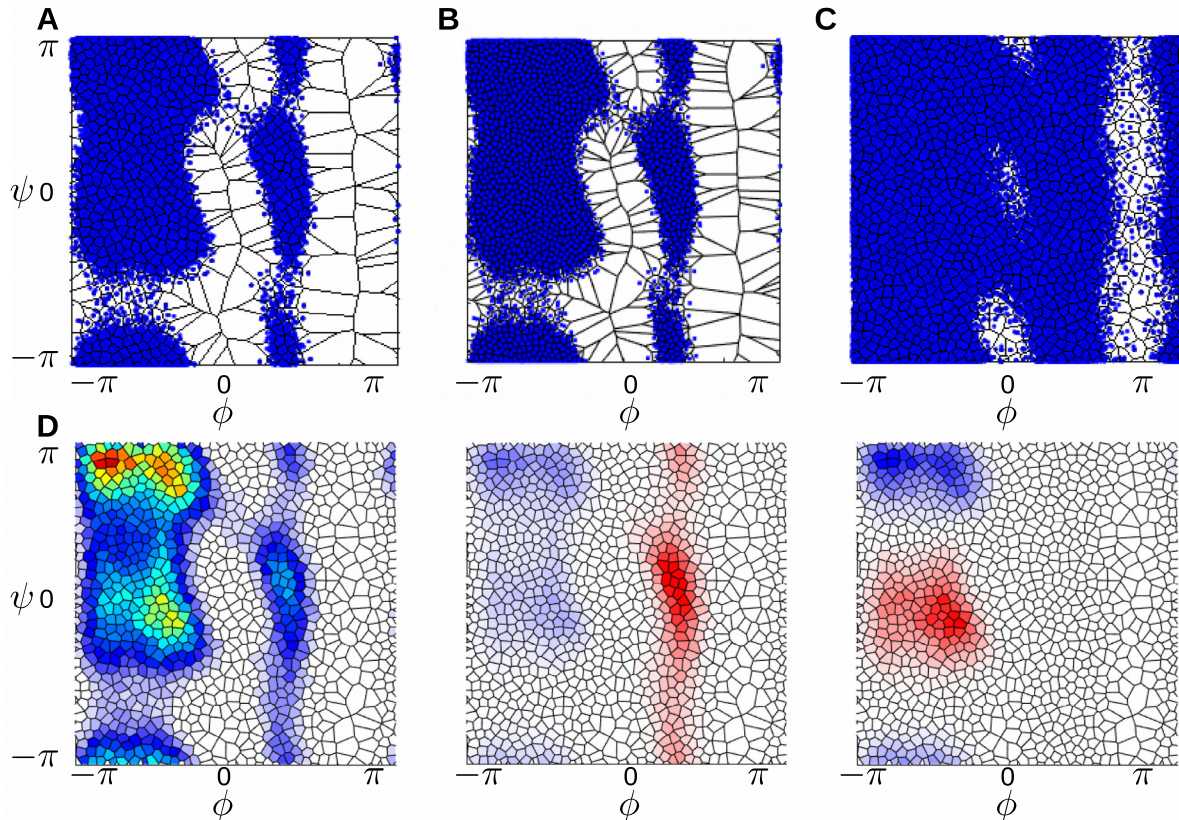


Figure 4. Alanine dipeptide. (A) Trajectory (ϕ_n, ψ_n) generated at temperature 300 K, Voronoi tessellation with $r = 0.17$. (B) Trajectory (ϕ_n, ψ_n) generated at temperature 300 K, Voronoi tessellation with $r = 0.1$. (C) Trajectory (ϕ_n, ψ_n) generated at temperature 900 K, Voronoi tessellation with $r = 0.17$. (D) First three left eigenvector of the rate matrix.

Table 7. Alanine dipeptide. Variation of the flux as function of the temperature (T) and the parameter r .

T (K)	r	ncells	$\hat{\Phi}_2$	$\hat{\Phi}_3$	$\bar{\Phi}$	std	rel. err. (%)
900	0.20	740	11.4390	12.9166	12.1778	1.0448	8.58
900	0.17	1005	17.0914	16.5862	16.8388	0.3572	2.12
300	0.17	566	0.1238	2.5672	1.3455	1.7277	128.41
300	0.14	792	0.1645	3.0356	1.6000	2.0301	126.88
300	0.10	1423	0.3090	6.4278	3.3684	4.3266	128.45

profile, higher-order reweighting schemes can be applied as well [40].

To estimate the value of the flux, we have constructed a MSM and the conformation matrices assuming the existence of three metastable states (β -sheet, $L\alpha$ -helix and $R\alpha$ -helix). Using a free energy profile obtained from a simulation at $T = 900$ K, the gap between $\hat{\Phi}_2$ and $\hat{\Phi}_3$ is statistically acceptable. If the Voronoi tessellation is built with $r = 0.2$, the error was 8.58% (table 7, first row). Reducing the size of the cells ($r = 0.17$), the error reduces to 2%, confirming the results obtained also for the two dimensional system (table 7, second row).

By contrast, if the free energy was obtained from a simulation at temperature $T = 300$ K, the difference between $\hat{\Phi}_2$ and $\hat{\Phi}_3$ is not negligible. The relative error is greater than 100%, and reducing the size of the cells ($r = 0.17, 0.14$ and 0.1) does not improve significantly the result (table 7, third, fourth and fifth rows). The reason for these results is that an insufficient sampling leads to an inhomogeneous Voronoi tessellation.

6. Conclusion

The paper contributes to the classical molecular simulation community in three ways. It provides an easy way to estimate the rates between metastable molecular conformations. It shows that this type of discretization converges to a Fokker–Planck operator. Finally, it shows that there is an easy mathematical relation between the discretized generator of the molecular process and the potential energy landscape.

For many years the concept of transfer operator, well known in thermodynamics and quantum mechanics, has been established inside the classical molecular simulation community [1–3] and new methods, such as Markov state models [1–9] have been developed to provide a discretized version of the transfer operator, in order to reduce the complexity and study conformational transition networks of molecular systems. The concept of transfer operator is connected to the concept of generator, which is simply the time-derivative of the transfer operator. While the spatial discretization of

the transfer operator is a transition probability matrix of a Markov chain, the spatial discretization of the generator is a rate matrix, which is, in general, hard to extract from time-discretized simulation data.

Our method simply uses the Boltzmann distribution of states for discretize the generator. The first underlying assumption is that we can define a continuity equation for the time-derivative of the transfer operator. Then, exploiting the Gauss theorem, we write the rate between two neighbor states as a surface integral of the flux, weighted by the Boltzmann density of the intersecting surface. The second assumption is a constant flux, i.e. the flux does not depend on the potential energy but on the discretization of the space. Instead of computing the Boltzmann weight of the intersecting surface of two adjacent Voronoi cells, here, it is estimated as geometric average of the Boltzmann weight of the cells. This we denoted as square root approximation (SQRA).

After having described in detail how to derive the SQRA, we have provided a mathematical proof that the rate matrix converges to the generator of the Smoluchowski equation [19] for infinitely small subsets of the conformational space. The validity of the theoretical assumptions has been confirmed also by numerical experiments. We have seen that the error on the measure of the flux decreases, reducing the size of the Voronoi cells, i.e. that the quality of the SQRA depends on the discretization of the state space. Moreover, we have demonstrated that an external perturbation to the potential energy function does not affect the value the flux, according to the second assumption about the independence of the flux on the potential energy function.

While for low dimensional systems, the SQRA can be linked directly to the potential energy function of the system; for high dimensional systems it is convenient to reduce the dimensionality to relevant coordinates and to replace the potential energy function with a free energy profile in few dimensions. In this paper, for alanine dipeptide, we have performed MD simulations at different temperatures in order to produce a discretized trajectories of the system. Afterward, we have recovered the free energy profile from the histogram of the trajectories projected on the backbone dihedral angles. The results have shown that the quality of the SQRA improves using the free energy profile built from the simulation realized at high temperature, which provides a better sampling of the state space.

The SQRA can be improved implementing enhanced sampling techniques like metadynamics [41, 42] or umbrella sampling [43], which offer a double advantage. Firstly, the MD simulation time is notably reduced; secondly, they provide an analytical function for the free energy profile.

An important further application of the square root approximation, is the possibility to study the effect of Hamiltonian perturbation on the dynamics of molecular systems. Like other reweighting methods [44], SQRA can be useful to improve the parametrization of force fields [25] or to test the influence of restraining potentials [45, 46] on the dynamics of the system. Furthermore, the method can be used to study the sensitivity

of the dominant eigenspace on the degrees of freedom of the system [47, 48].

In conclusion, we believe that the square root approximation can become a fundamental tool for the study of the dynamics of molecular systems and can expands its borders of applicability in different ways that will be treated in future works.

Acknowledgments

This research has been funded by Deutsche Forschungsgemeinschaft (DFG) through grant CRC 1114 *Scaling Cascades in Complex Systems*, Projects A05 *Probing scales in equilibrated systems by optimal nonequilibrium forcing*, B05 *Origin of the scaling cascades in protein dynamics* and C05 *Effective models for interfaces with many scales*.

Appendix A. Gauss theorem

The Gauss theorem can be used to rewrite the non-diagonal entries of the matrix \mathbf{Q} as a function of the flux and the stationary distribution.

A.1. Gauss theorem

Given a Voronoi tessellation of the state space $\Gamma = \cup_{i=1}^n \Omega_i$ and the discretized transfer operator $\mathbf{T}(\tau)$, the matrix

$$\mathbf{Q} := \left. \frac{\partial \mathbf{T}(\tau)}{\partial \tau} \right|_{\tau=0} \text{ satisfies} \quad Q_{ij} = \frac{1}{\pi_i} \oint_{\partial\Omega_i \partial\Omega_j} \Phi(\mathbf{z}) \pi(\mathbf{z}) dS(\mathbf{z}) \quad (\text{A.1})$$

where $\partial\Omega_i \partial\Omega_j$ is the common surface between the cell Ω_i and Ω_j , π_i is the Boltzmann density of the cell i and $\Phi(\mathbf{z})$ denotes the flux of the configurations $\mathbf{z} \in \partial\Omega_i \partial\Omega_j$, through the infinitesimal surface $\partial\Omega_i \partial\Omega_j$.

A.2. Proof

The conditional probability density $p(\mathbf{x}, \mathbf{y}; \tau)$ denotes the probability of observing the system in the state \mathbf{y} , after a time τ , given that it has been in \mathbf{x} . Because the system will always assume a thermodynamic state, it yields $\int_{\Gamma} p(\mathbf{x}, \mathbf{y}; \tau) d\mathbf{y} = 1$. Thus, the conservation of the conditional probability density, can be associated to the mass conservation of a fluid, that moves in the state space Γ , transporting the properties of the system and we can introduce the continuity equation:

$$\left. \frac{\partial p(\mathbf{x}, \mathbf{y}; \tau)}{\partial \tau} \right|_{\tau=0} = -\nabla_{\mathbf{y}} \cdot \mathbf{j} \quad (\text{A.2})$$

where $\mathbf{j} = p(\mathbf{x}, \mathbf{y}; \tau) \mathbf{v}(\mathbf{x})$ is the density flux and $\mathbf{v}(\mathbf{x})$ is the flow velocity. We interpret the flux of the probability density as the probability per unit area per unit time, that a trajectory passes through a surface. While the flow velocity vector

represents the velocity with which the system moves from the state \mathbf{x} to \mathbf{y} .

We now use the continuity equation, to rewrite \mathbf{Q} :

$$\begin{aligned}
Q_{ij} &:= \left. \frac{\partial T_{ij}(\tau)}{\partial \tau} \right|_{\tau=0} \\
\text{(a)} &= \left. \frac{\partial}{\partial \tau} \left[\frac{1}{\pi_i} \int_{\Omega_j} \int_{\Omega_i} p(\mathbf{x}, \mathbf{y}; \tau) \pi(\mathbf{x}) d\mathbf{x} d\mathbf{y} \right] \right|_{\tau=0} \\
&= \frac{1}{\pi_i} \int_{\Omega_j} \int_{\Omega_i} \left. \frac{\partial p(\mathbf{x}, \mathbf{y}; \tau)}{\partial \tau} \right|_{\tau=0} \pi(\mathbf{x}) d\mathbf{x} d\mathbf{y} \\
\text{(b)} &= \frac{1}{\pi_i} \int_{\Omega_j} \int_{\Omega_i} -\nabla_{\mathbf{y}} \cdot \mathbf{j}|_{\tau=0} \pi(\mathbf{x}) d\mathbf{x} d\mathbf{y} \\
\text{(c)} &= \frac{1}{\pi_i} \int_{\Omega_j} \oint_{\partial\Omega_i} -\mathbf{j}|_{\tau=0} \cdot \mathbf{n}_i \pi(\mathbf{x}) dS(\mathbf{x}) d\mathbf{y} \\
\text{(d)} &= \frac{1}{\pi_i} \int_{\Omega_j} \oint_{\partial\Omega_i} -\delta_{\mathbf{x}=\mathbf{y}} \mathbf{v}(\mathbf{x}) \cdot \mathbf{n}_i \pi(\mathbf{x}) dS(\mathbf{x}) d\mathbf{y} \\
\text{(e)} &= \frac{1}{\pi_i} \oint_{\partial\Omega_i, \partial\Omega_j} \Phi(\mathbf{z}) \pi(\mathbf{z}) dS(\mathbf{z}) \quad (\text{A.3})
\end{aligned}$$

where we have used:

- (a) The discretized version of the transfer operator in equation (8).
- (b) The continuity equation.
- (c) The divergence theorem. The vector \mathbf{n}_i is the unit vector orthogonal to the surface $\partial\Omega_i$.
- (d) Because $\tau = 0$, we have

$$p(\mathbf{x}, \mathbf{y}; \tau) = \delta_{\mathbf{x}=\mathbf{y}}. \quad (\text{A.4})$$

Then the density flux is $\mathbf{j}|_{\tau=0} = \delta_{\mathbf{x}=\mathbf{y}} \mathbf{v}(\mathbf{x})$.

- (e) If $\tau = 0$, only instantaneous transitions between neighbor cells have to be taken into account. Thus, the only points that satisfy $\mathbf{x} = \mathbf{y}$, are the points on the intersecting surface $\partial\Omega_i, \partial\Omega_j$. The quantity $\Phi(\mathbf{z})$ denotes the flux of the configurations \mathbf{z} through the infinitesimal surface $\partial\Omega_i$. Note that $\Phi(\mathbf{z}) = -\delta_{\mathbf{x}=\mathbf{y}} \mathbf{v}(\mathbf{x}) \cdot \mathbf{n}_i = \delta_{\mathbf{x}=\mathbf{y}} \mathbf{v}(\mathbf{x}) \cdot \mathbf{n}_j$ where \mathbf{n}_j is the unit vector normal to the surface $\partial\Omega_j$.

□

Appendix B. Transition matrices in the space of conformations

In the following section, we explain why the relation $\exp(\tau \mathbf{Q}^c) = \mathbf{T}^c(\tau)$ (equation (38)) is true.

We consider a partition of the state-space Γ into n_c overlapping metastable conformations. We now introduce a set of n_c membership functions $\chi = \{\chi_1, \dots, \chi_{n_c}\}$ such that the function $\chi_i(\mathbf{x}) : \Gamma \rightarrow [0, 1]$ provides the probability that a state $\mathbf{x} \in \Gamma$ belongs to the conformation C_i : The membership functions meet the partition of unity property, i.e. $\forall \mathbf{x} \in \Gamma, \sum_i^{n_c} \chi_i(\mathbf{x}) = 1 \forall i$. Thus the membership functions determine a standard n_c -simplex.

Because of metastability of the conformations, a state \mathbf{x} tends to not leave its starting conformation C_i . Thus, the

product between the generator \mathbf{Q} and the membership function χ_i is almost zero for each conformation i :

$$\mathbf{Q}\chi_i \approx 0 \quad \forall i = 1, \dots, n_c. \quad (\text{B.1})$$

For the identification of the conformations, it can be assumed, that the function χ_i spans the same linear space as the leading first n_c right eigenfunctions \mathcal{F}_i of the generator \mathbf{Q} , associated to eigenvalues θ_i near zero [31]. Thus, we can define an invertible transformation matrix \mathbf{A} of size $n_c \times n_c$, such that $\chi = \mathcal{F}\mathbf{A}$, then

$$\mathbf{Q}(\mathcal{F}\mathbf{A})_i = \theta_i(\mathcal{F}\mathbf{A})_i \approx 0. \quad (\text{B.2})$$

The transformation matrix \mathbf{A} is finally used to prove that if \mathbf{Q} is the infinitesimal generator of $\mathcal{T}(\tau)$, then \mathbf{Q}^c is the generator of $\mathbf{T}^c(\tau)$.

B.1. Lemma [49, 50]

If the n_c eigenfunctions $\mathcal{F} = \{\mathcal{F}_1, \dots, \mathcal{F}_{n_c}\}$ of \mathbf{Q} , associated to eigenvalues $\theta_i \approx 0$, are π -orthonormal and $\chi = \mathcal{F}\mathbf{A}$ is a regular basis transformation of these eigenfunctions, then

$$\text{if } \exp(\tau \mathbf{Q}) = \mathcal{T}(\tau) \Rightarrow \exp(\tau \mathbf{Q}^c) = \mathbf{T}^c(\tau).$$

Proof. The eigenfunctions \mathcal{F}_i of \mathbf{Q} are eigenfunctions also of $\mathcal{T}(\tau)$ with eigenvalues $\lambda_i(\tau) = \exp(\tau \theta_i)$ (semigroup property). Thus it yields

$$\begin{aligned}
\mathcal{T}(t)\mathcal{F}_i &= \lambda_i(\tau)\mathcal{F}_i = \exp(\tau \theta_i)\mathcal{F}_i \\
\mathbf{Q}\mathcal{F}_i &= \theta_i \mathcal{F}_i. \quad (\text{B.3})
\end{aligned}$$

The matrix $\mathbf{T}^c(\tau)$ of the conformations is the Galerkin discretization of the operator $\mathcal{T}(\tau)$ on the basis of the membership functions χ_i . Since the membership functions are not orthogonal, the matrix $\mathbf{T}^c(\tau)$ is the product of two matrices generated by the corresponding inner products:

$$\mathbf{T}^c(\tau) = (\langle \chi, \chi \rangle_{\pi})^{-1} \langle \chi, \mathcal{T}(\tau) \chi \rangle_{\pi}. \quad (\text{B.4})$$

Replacing $\chi = \mathcal{F}\mathbf{A}$ in equation (B.4), then

$$\begin{aligned}
\mathbf{T}^c(\tau) &= (\langle \chi, \chi \rangle_{\pi})^{-1} \langle \chi, \mathcal{T}(\tau) \chi \rangle_{\pi} \\
&= (\mathbf{A}^{\top} \langle \mathcal{F}^{\top}, \mathcal{F} \rangle_{\pi} \mathbf{A})^{-1} \mathbf{A}^{\top} \langle \mathcal{F}^{\top}, \mathcal{T}(\tau) \mathcal{F} \rangle_{\pi} \mathbf{A} \\
&= (\mathbf{A}^{\top} \mathbf{A})^{-1} \mathbf{A}^{\top} \langle \mathcal{F}^{\top}, \Lambda(\tau) \mathcal{F} \rangle_{\pi} \mathbf{A} \\
&= \mathbf{A}^{\top} \langle \mathcal{F}^{\top}, \mathcal{F} \rangle_{\pi} \Lambda(\tau) \mathbf{A} \\
&= \mathbf{A}^{\top} \Lambda(\tau) \mathbf{A}. \quad (\text{B.5})
\end{aligned}$$

It follows that

$$\begin{aligned}
\mathbf{T}^c(\tau) &= \mathbf{A}^{\top} \Lambda(\tau) \mathbf{A} \\
&= \mathbf{A}^{\top} \exp(\tau \Theta) \mathbf{A} \\
&= \exp(\tau \mathbf{Q}^c) \quad (\text{B.6})
\end{aligned}$$

where the matrices Θ and $\Lambda(\tau)$ denote respectively the diagonal matrices $n_c \times n_c$ of the eigenvalues θ_i and $\lambda(\tau)_i$. Then \mathbf{Q}^c is an infinitesimal generator of $\mathbf{T}^c(\tau)$. □

In practice, one can exploit the partition of unity property to determine the transformation matrix \mathbf{A} using the Robust Perron cluster analysis (PCCA+) [26]. The eigenfunctions \mathcal{F} are unknown, thus one can use the eigenvectors of the matrix \mathbf{Q} estimated by square root approximation.

ORCID iDs

Luca Donati  <https://orcid.org/0000-0002-6014-6875>
 Martin Heida  <https://orcid.org/0000-0002-7242-8175>
 Bettina G Keller  <https://orcid.org/0000-0002-7051-0888>

References

- [1] Schütte C, Fischer A, Huisinga W and Deuffhard P 1999 *J. Comput. Phys.* **151** 146
- [2] Schütte C, Huisinga W and Deuffhard P 2001 Transfer operator approach to conformational dynamics in biomolecular systems *Ergodic Theory, Analysis, and Efficient Simulation of Dynamical Systems* ed B Fiedler (Berlin: Springer) pp 191–223
- [3] Prinz J-H, Wu H, Sarich M, Keller B, Senne M, Held M, Chodera J D, Schütte C and Noé F 2011 *J. Chem. Phys.* **134** 174105
- [4] Deuffhard P, Huisinga W, Fischer A and Schütte C 2000 *Linear Algebr. Appl.* **315** 39
- [5] Swope W C, Pitera J W and Suits F 2004 *J. Phys. Chem. B* **108** 6571
- [6] Chodera J D, Singhal N, Pande V S, Dill K A and Swope W C 2007 *J. Chem. Phys.* **126** 155101
- [7] Buchete N-V and Hummer G 2008 *J. Phys. Chem. B* **112** 6057
- [8] Keller B, Daura X and Van Gunsteren W F 2010 *J. Chem. Phys.* **132** 074110
- [9] Keller B, Hünenberger P and van Gunsteren W F 2011 *J. Chem. Theory Comput.* **7** 1032
- [10] Lemke O and Keller B G 2016 *J. Chem. Phys.* **145** 164104
- [11] Nüske F, Keller B, Perez-Hernandez G, Mey A S J S and Noé F 2014 *J. Chem. Theory Comput.* **10** 1739
- [12] Voelz V A, Bowman G R, Beauchamp K A and Pande V S 2010 *J. Am. Chem. Soc.* **132** 1526
- [13] Fabritiis G D, Stanley N and Esteban-Martín S 2014 *Nat. Commun.* **5** 5272
- [14] Bowman G R, Bolin E R, Hart K M, Maguire B C and Marqusee S 2015 *Proc. Natl Acad. Sci. USA* **112** 2734
- [15] Plattner N and Noé F 2015 *Nat. Commun.* **6** 7653
- [16] Zhang L, Unarta I C, Cheung P P-H, Wang G, Wang D and Huang X 2016 *Acc. Chem. Res.* **49** 687
- [17] Witek J, Keller B G, Blatter M, Meissner A, Wagner T and Riniker S 2016 *J. Chem. Inf. Model.* **56** 1547
- [18] Øksendal B 2003 *Stochastic Differential Equations: an Introduction with Applications* 6th edn (Berlin: Springer) (<https://doi.org/10.1007/978-3-642-14394-6>)
- [19] Heida M 2018 *Math. Models Methods Appl. Sci.* accepted (<https://doi.org/10.1142/S0218202518500562>)
- [20] Bicout D J and Szabo A 1998 *J. Chem. Phys.* **109** 2325
- [21] Lie H C, Fackeldey K and Weber M 2013 *SIAM. J. Matrix Anal. Appl.* **34** 738
- [22] Schild A 2013 Electron fluxes during chemical processes in the electronic ground state *PhD Thesis Freie Universität Berlin* www.diss.fu-berlin.de/diss/receive/FUDISS_thesis_000000095279
- [23] Dixit P D, Jain A, Stock G and Dill K A 2015 *J. Chem. Theory Comput.* **11** 5464
- [24] Vymětal J and Vondrášek J 2010 *J. Phys. Chem. B* **114** 5632
- [25] Vitalini F, Mey A S J S, Noé B G, Keller F, Vitalini F, Mey A S J S, Noé F and Keller B G 2015 *J. Chem. Phys.* **142** 084101
- [26] Deuffhard P and Marcus W 2004 *Linear Algebr. Appl.* **398** 161
- [27] Bouchaud J-P and Georges A 1990 *Phys. Rep.* **195** 127
- [28] Biskup M 2011 *Probab. Surv.* **8** 294
- [29] Jikov V V, Kozlov S M and Oleĭnik O A 1994 *Homogenization of Differential Operators and Integral Functionals* (Berlin: Springer) (translated from the Russian by G A Yosifian (G A Iosif'yan)) (<https://doi.org/10.1007/978-3-642-84659-5>)
- [30] Alicandro R, Cicalese M and Gloria A 2011 *Arch. Ration. Mech. Anal.* **200** 881
- [31] Weber M 2011 A subspace approach to molecular Markov state models via a new infinitesimal generator *Habilitation Thesis Freie Universität Berlin, Zuse Institute Berlin* (<http://nbn-resolving.de/urn:nbn:de:0297-zib-14025>)
- [32] Kube S and Weber M 2008 *AIP Conf. Proc.* **1048** 593
- [33] Fukuda K 2004 Frequently asked questions in polyhedral computation (www.cs.mcgill.ca/~fukuda/soft/polyfaq/node1.html)
- [34] Bowman G R, Pande V S and Noé F (ed) 2014 *An Introduction to Markov State Models and their Application to Long Timescale Molecular Simulation (Advances in Experimental Medicine and Biology vol 797)* (Heidelberg: Springer) (<https://doi.org/10.1007/978-94-007-7606-7>)
- [35] Van Der Spoel D, Lindahl E, Hess B, Groenhof G, Mark A E and Berendsen J H 2005 *J. Comput. Chem.* **26** 1701
- [36] Lindorff-Larsen K, Piana S, Palmo K, Maragakis P, Klepeis J, Dror R and Shaw E D 2010 *Proteins* **78** 1950
- [37] Jorgensen W L, Chandrasekhar J, Madura J D, Impey R W and Klein M 1983 *J. Chem. Phys.* **79** 926
- [38] Bussi G, Donadio D and Parrinello M 2007 *J. Chem. Phys.* **126** 014101
- [39] Hockney R W, Goel S P and Eastwood J 1974 *J. Comput. Phys.* **14** 148
- [40] Durmaz V, Fackeldey K and Weber M 2011 A rapidly-mixing monte carlo method for the simulation of slow molecular processes *Applications of Monte Carlo Methods in Biology, Medicine and Other Fields of Science* ed C J Mode (London: Intech Open) ch 11, pp 399–424
- [41] Huber T, Torda A E and van Gunsteren W F 1994 *J. Comput. Aided Mol. Des.* **8** 695
- [42] Laio A and Parrinello M 2002 *Proc. Natl Acad. Sci. USA* **99** 12562
- [43] Torrie G and Valleau J 1977 *J. Comput. Phys.* **23** 187
- [44] Donati L, Hartmann C and Keller B G 2017 *J. Chem. Phys.* **146** 244112
- [45] Cesari A, Gil-Ley A and Bussi G 2016 *J. Chem. Theory Comput.* **12** 6192
- [46] Keller B, Christen M, Oostenbrink C and Van Gunsteren W F 2007 *J. Biomol. NMR* **37** 1
- [47] Tsourtis A, Pantazis Y, Katsoulakis M and Harmandaris V 2015 *J. Chem. Phys.* **143** 014116
- [48] Arampatzisa G, Katsoulakis M and Rey-Bellet L 2016 *J. Chem. Phys.* **144** 104107
- [49] Kube S and Weber M 2006 *ZIB Report ZR-06-35* (<http://nbn-resolving.de/urn:nbn:de:0297-zib-9299>)
- [50] Weber M 2009 *ZIB Report ZR-09-27* (<http://nbn-resolving.de/urn:nbn:de:0297-zib-11432>)